

A Stability Model for Transonic Axial Compressors

Weiwei Yu¹ and Xiaofeng Sun²

¹Department of Aeroengine
Beijing University of Aeronautics and Astronautics
37 Xueyuan Road, Beijing 100083, CHINA

Phone: +86-10-8231-6337, FAX: +86-10-8232-9401, E-mail: yww407@yahoo.com.cn

²Department of Aeroengine
Beijing University of Aeronautics and Astronautics

ABSTRACT

The stability theory of rotating stall of compressors is to help understanding the mechanism of rotating stall in order to find various ways to extend the stall margin. To transonic axial flow compressors or fans, there is very few models to discuss the effect of the presence of a strong in-passage shocks on the stability. Based on an existing compressible three-dimensional rotating stall stability model, the effect of shock is included in the present theory. Some calculations are carried out and the relevant results are compared with an experimental data of a transonic stage. In fact, this model shows that it is very important to include the effect of a strong in-passage shock in a blade row to the compressor stability prediction .

Nomenclature

Variables

α	axial wave number
β	relative flow angle
θ	stagger angle of blade row
ρ	density
ω	angular frequency of disturbance wave
a	sound speed
L	loss
M	Mach number
p	pressure
q	disturbance velocity of channel flow
r_m	mean radius
u	axial velocity
v	circumferential velocity
w	radial velocity
W	mean flow velocity of channel
Ω	Rotor speed
Superscript	
a	region upstream of shock
b	region downstream of shock
j	index of unbladed region
k	index of bladed region

Subscript

0	average
m	circumferential mode number
n	radial mode number
s	shock
p	acoustic
v	vortical or entropic

Introduction

Considerable work was done in the past several decades on investigating the phenomenon of rotating stall in axial flow compressors. The overall objective of these theories was to predict inception conditions and identify the fundamental mechanism involved.

Takata and Nagano(1970) developed a nonlinear model to analysis rotating stall, which emphasize the role of the nonlinear aspects in determining the propagation velocity and do not identify the fundamental mechanisms that produce rotating stall. Nenni and Ludwig(1974) extended the channel flow theory presented by Sears(1955) to include the effects of more geometrical and aerodynamic parameters of compressor. The work was soon extended to two dimensional compressible flow case(Ludwig, 1979). Greitzer(1976) and Moore(1984,1986) presented stability model of compressor in different approach. The model can not only be used to predict the inception condition of stall and surge but also to study the non-linear development of stall cells. The compressible flow stability model of rotating stall in multi-stage compressors are also investigated based on solving linearized Euler equations(Feulner, 1994). However, all of these work are based on the assumption that flow is two-dimensional. There were some attempts to set up three-dimensional compressible stability model of compressor in the previous work. Ludwig(1979) and Nenni developed a three-dimensional incompressible flow stability model of rotating stall but no any numerical results were presented. Takata and Nagashima(1985) studied the rotating stall in three-dimensional blade rows with emphasis on the effect of non-uniform flow or shear flow on the stall inception. Sun(1996) developed a three-dimensional compressible stability model of rotating stall to include the effect of boundary condition of casing treatment.

For advanced gas turbine engines, transonic axial flow compressors or fans have been widely used. Compared to subsonic compressors, transonic compressors face more severe restrictions on the stall margin. However, there is little knowledge of stability prediction for transonic compressors.

In fact, the existing compressible stability models of rotating stall mainly aim at the stability prediction for subsonic flow. Therefore, it is still not known that how a strong in-passage shock in a blade row affects the stability of a compressor. The complex nature of this issue has thus far resisted rigorous mathematical formulation, but a "simplified" model has been undertaken herein based on a modified semi-actuator disk approach with channel flow. A similar method had been employed by Adamzyk(1978) and Micklow(1981) on researching supersonic bending flutter in axial flow compressors.

The present theory is a natural extension of the model developed by Sun(1996). As all the previous small perturbation theories of rotating stall have been, the blade row performance data need to be fed into model. At present, the source of these data could be from experiment or numerical calculation. In the following sections, this model will be described in detail and then some numerical results will be discussed for further understanding the mechanism of rotating stall in transonic axial flow compressors or fans.

Stability Model

This rotating stall stability model was based on small disturbance assumption. It was developed to investigate the stability of compressible flow in high-speed multi-stage axial flow compressors. It was envisaged that the model would be used for the analysis of the effects of loss of rows and the existence of shock in supersonic condition. This model separates compressors into unbladed regions and bladed regions as shown in Fig.(1). It is also assumed that the radius of hub and casing of compressor will keep constant in each separated flowfields but will be different with each other.

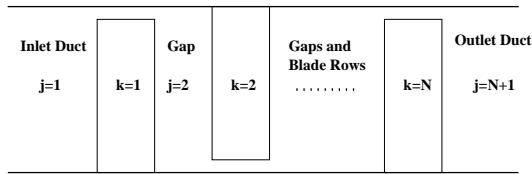


Fig.1: Multi-Row Axial Flow Compressor

It is unlike some incompressible stability theories, the mean flow in this theory would vary in different sections. But it was assumed that mean flow velocity was zero in radial direction. Although the radial main flow was ignored, radial unsteady velocity would be included in the stability model. Three dimensional unsteady linearized Euler equations were used in unbladed region and two dimensional equations in blade rows. The unsteady flow field is presented by pressure perturbation, velocity perturbations and density perturbation. Matching conditions would be used to combine solutions together at shock wave, leading edge and trailing edge of each blade row, then one homogeneous stability equation could be set up. Further the frequency of the rotating stall waves could be obtained by solving this equations, which generally consists of an real part and an imaginary part, i.e.

$$\omega = \omega_r + i\omega_i \quad (1)$$

The flow is neutrally stable if $\omega_i = 0$, unstable if $\omega_i < 0$ and stable $\omega_i > 0$.

Solution in Unbladed Regions

Unbladed Regions comprised inlet duct, gaps between successive blade rows and the exit duct. The linearized Euler

equations applied to gaps and ducts are in Cartesian coordinates, which are as follows:

$$\begin{aligned} \frac{\partial p}{\partial t} + U \frac{\partial p}{\partial x} + V \frac{\partial p}{\partial y} + \rho \left(\frac{\partial u}{\partial x} + \frac{\partial v}{\partial y} + \frac{\partial w}{\partial z} \right) &= 0 \\ \frac{\partial u}{\partial t} + U \frac{\partial u}{\partial x} + V \frac{\partial u}{\partial y} &= -\frac{1}{\rho_0} \frac{\partial p}{\partial x} \\ \frac{\partial v}{\partial t} + U \frac{\partial v}{\partial x} + V \frac{\partial v}{\partial y} &= -\frac{1}{\rho_0} \frac{\partial p}{\partial y} \\ \frac{\partial w}{\partial t} + U \frac{\partial w}{\partial x} + V \frac{\partial w}{\partial y} &= -\frac{1}{\rho_0} \frac{\partial p}{\partial z} \\ \frac{1}{P_0} \frac{\partial p}{\partial t} + U \frac{\partial p}{\partial x} + V \frac{\partial p}{\partial y} - \frac{\kappa}{\rho_0} \left(\frac{\partial p}{\partial t} + U \frac{\partial p}{\partial x} + V \frac{\partial p}{\partial y} \right) &= 0 \end{aligned} \quad (2)$$

From Equations.2, it can be shown that fluctuating variables related to pressure will satisfy the wave equation in the form of

$$\begin{aligned} (1 - M_x^2) \frac{\partial^2 p}{\partial x^2} + (1 - M_y^2) \frac{\partial^2 p}{\partial y^2} - 2M_x M_y \frac{\partial^2 p}{\partial x \partial y} + \frac{\partial^2 p}{\partial z^2} \\ - \frac{1}{a_0^2} \frac{\partial^2 p}{\partial t^2} - 2M_x \frac{1}{a_0} \frac{\partial^2 p}{\partial x \partial t} - 2M_y \frac{1}{a_0} \frac{\partial^2 p}{\partial y \partial t} = 0 \end{aligned} \quad (3)$$

where, M_x and M_y represent axial and circumferential Mach number, respectively.

A general method of solving partial derivative equations is to use a transform or series expansion to eliminate derivatives with respect to independent variables. Assuming the solution of unsteady Euler equations has a Fourier series form in the circumferential direction, $e^{i\beta m}$, and a complex exponential, $e^{i\omega t}$. Where,

$$\beta m = \frac{m}{r_m}$$

$$\omega = \omega_r + i\omega_i$$

. Integer m means the circumferential mode number and n means radial mode number. For radial mode, there are some discussion in reference(Sun, 1996), in which the radial wave number is related to boundary condition at hub and casing. In this paper, hard wall boundary condition was adopted. Therefore the radial wave number k_m is $\frac{(n-1)\pi}{h}$, where n is radial mode number and h is the height from the hub to tip. Accordingly, the eigenfunction of radial direction can be written as:

$$\psi(z) = \cos k_m n z \quad (4)$$

Unsteady pressure perturbation wave has a form as:

$$p(x, y, z, t) = \sum_{m=-\infty}^{+\infty} p_{mn}(x) \psi_{mn}(z) e^{i(\omega t + \beta_m y)} \quad (5)$$

Substituting it into Eq.(3) the result is one complex constant coefficient ordinary derivative equation(ODE) in x for each mode.

$$\begin{aligned} (1 - M_x^2) \frac{\partial^2 p_{mn}}{\partial x^2} - 2iM_x \left(M_y \beta_m + \frac{\omega}{a_0} \right) \frac{\partial p_{mn}}{\partial x} \\ + [(\beta^2 + k_{mn}^2) + \left(M_y \beta_m + \frac{\omega}{a_0} \right)^2] p_{mn} = 0 \end{aligned} \quad (6)$$

This can be solved by assuming exponential in x and solving for the complex exponential constants:

$$p_{mn}(x) = \bar{p}_{mn} e^{i\alpha_{mn}(x-x^j)}$$

Where α is axial wave number. Substituting the upper form of solution of pressure into Eq.(6) yields

$$\begin{aligned} \alpha_{mn}^{+j} &= \frac{M_x \left(M_y \beta_m + \frac{\omega}{a_0} \right) + \sqrt{\left(M_y \beta_m + \frac{\omega}{a_0} \right)^2 - (1 - M_x^2) (\beta_m^2 + (k_{mn}^+)^2)}}{1 - M_x^2} \\ \alpha_{mn}^{-j} &= \frac{M_x \left(M_y \beta_m + \frac{\omega}{a_0} \right) - \sqrt{\left(M_y \beta_m + \frac{\omega}{a_0} \right)^2 - (1 - M_x^2) (\beta_m^2 + (k_{mn}^-)^2)}}{1 - M_x^2} \end{aligned} \quad (7)$$

Finally the pressure can be expressed as

$$p(x, y, z, t) = \sum_{m=-\infty}^{+\infty} \sum_{n=1}^{+\infty} (\bar{p}_{mn}^{+j} \psi_{mn}^{+j}(z) e^{i\alpha_{mn}^{+j}(x-x^j)} + \bar{p}_{mn}^{-j} \psi_{mn}^{-j}(z) e^{i\alpha_{mn}^{-j}(x-x^j)}) e^{i(\omega t + \beta_m y)} \quad (8)$$

In this expression the two components represent two Riemann sheets of the solution separated by branch cuts arising from the square root of the complex frequency parameter, ω . Physically, they mean downward and fore-ward propagating wave from the plane x^j . Imaginary part of ω is damping factor which determines whether the amplitude will decay or magnify from plane x^j . \bar{p}_{mn}^{+j} and \bar{p}_{mn}^{-j} are two unknown coefficients which determine the amplitude of the disturbance.

According to velocity splitting theorem, the fluctuating velocity can be decomposed into acoustic mode related to pressure variation and vortical mode as follows:

$$\begin{cases} w^j(x, y, z, t) = u_p^j + u_v^j \\ v^j(x, y, z, t) = v_p^j + v_v^j \\ w^j(x, y, z, t) = w_p^j + w_v^j \end{cases} \quad (9)$$

Similarly, density disturbance is split into acoustic mode and entropy mode, which are related through energy equation. The density is represented as follows:

$$\rho^j(x, y, z, t) = \rho_p^j + \rho_v^j \quad (10)$$

Substituting solution of pressure into Euler equations and energy equations yields solution of velocity and density in a very similar form of pressure.

$$\begin{aligned} \rho(x, y, z, t) &= \sum_{m=-\infty}^{+\infty} \sum_{n=1}^{+\infty} \left[\frac{1}{a_0^2} (\bar{p}_{mn}^{+j} \psi_{mn}^{+j}(z) e^{i\alpha_{mn}^{+j}(x-x^j)} + \bar{p}_{mn}^{-j} \psi_{mn}^{-j}(z) e^{i\alpha_{mn}^{-j}(x-x^j)}) \right. \\ &\quad \left. + \bar{\rho}_{vmn}^{+j} \psi_{vmn}^{+j}(z) e^{-i\frac{\omega+V^j\beta_m}{U^j}(x-x^j)} \right] e^{i(\beta_m y + \omega t)} \\ u(x, y, z, t) &= \sum_{m=-\infty}^{+\infty} \sum_{n=1}^{+\infty} \left[-\frac{1}{\rho_0^j} \left(\frac{\bar{p}_{mn}^{+j} \alpha_{mn}^{+j} e^{i\alpha_{mn}^{+j}(x-x^j)}}{\omega + \alpha_{mn}^{+j} U^j + \beta_m V^j} \psi_{mn}^{+j}(z) \right. \right. \\ &\quad \left. \left. + \frac{\bar{p}_{mn}^{-j} \alpha_{mn}^{-j} e^{i\alpha_{mn}^{-j}(x-x^j)}}{\omega + \alpha_{mn}^{-j} U^j + \beta_m V^j} \psi_{mn}^{-j}(z) \right) \right. \\ &\quad \left. + \bar{u}_{vmn}^{+j} \psi_{vmn}^{+j}(z) e^{-i\frac{\omega+V^j\beta_m}{U^j}(x-x^j)} \right] e^{i(\beta_m y + \omega t)} \\ v(x, y, z, t) &= \sum_{m=-\infty}^{+\infty} \sum_{n=1}^{+\infty} \left[-\frac{1}{\rho_0^j} \left(\frac{\bar{p}_{mn}^{+j} \beta_m^{+j} e^{i\alpha_{mn}^{+j}(x-x^j)}}{\omega + \alpha_{mn}^{+j} U^j + \beta_m V^j} \psi_{mn}^{+j}(z) \right. \right. \\ &\quad \left. \left. + \frac{\bar{p}_{mn}^{-j} \beta_m^{-j} e^{i\alpha_{mn}^{-j}(x-x^j)}}{\omega + \alpha_{mn}^{-j} U^j + \beta_m V^j} \psi_{mn}^{-j}(z) \right) \right. \\ &\quad \left. + \bar{v}_{vmn}^{+j} \psi_{vmn}^{+j}(z) e^{-i\frac{\omega+V^j\beta_m}{U^j}(x-x^j)} \right] e^{i(\beta_m y + \omega t)} \\ w(x, y, z, t) &= \sum_{m=-\infty}^{+\infty} \sum_{n=1}^{+\infty} \left[-\frac{1}{\rho_0^j} \left(\frac{\bar{p}_{mn}^{+j} k_{mn}^{+j} e^{i\alpha_{mn}^{+j}(x-x^j)}}{\omega + \alpha_{mn}^{+j} U^j + \beta_m V^j} \phi_{mn}^{+j}(z) \right. \right. \\ &\quad \left. \left. + \frac{\bar{p}_{mn}^{-j} k_{mn}^{-j} e^{i\alpha_{mn}^{-j}(x-x^j)}}{\omega + \alpha_{mn}^{-j} U^j + \beta_m V^j} \phi_{mn}^{-j}(z) \right) \right. \\ &\quad \left. + \bar{w}_{vmn}^{+j} \phi_{vmn}^{+j}(z) e^{-i\frac{\omega+V^j\beta_m}{U^j}(x-x^j)} \right] e^{i(\beta_m y + \omega t)} \end{aligned} \quad (11)$$

Solution in Bladed Region

The impact of rotor rows and stator rows were substituted by three-dimensional semi-actuator disks. This means that the main flow in the blade rows is treated as one-dimensional. But there are radial fluctuating velocity component and chord wise fluctuating velocity component. So the two-dimensional unsteady Euler equations describing the

three-dimensional semi-actuator disk are

$$\begin{aligned} \frac{\partial \rho}{\partial t} + W \frac{\partial \rho}{\partial \xi} + \rho_0 \left(\frac{\partial q}{\partial \xi} + \frac{\partial w}{\partial z} \right) &= 0 \\ \frac{\partial q}{\partial t} + W \frac{\partial q}{\partial \xi} &= -\frac{1}{\rho_0} \frac{\partial p}{\partial \xi} \\ \frac{\partial w}{\partial t} + W \frac{\partial w}{\partial \xi} &= -\frac{1}{\rho_0} \frac{\partial p}{\partial z} \\ \frac{1}{\rho_0} \left(\frac{\partial p}{\partial t} + W \frac{\partial p}{\partial \xi} \right) - \frac{\kappa}{\rho_0} \left(\frac{\partial \rho}{\partial t} + W \frac{\partial \rho}{\partial \xi} \right) &= 0 \end{aligned} \quad (12)$$

For this equations the coordinate is fixed to the blade row and ξ is along the channel direction. Besides it should be noted that in the phase change of the wave motion in the cascade direction must coincide with that in the upstream or downstream flow. Therefore the solution of the perturbation waves along the ξ direction should be sought in the form $e^{i(\omega t + \beta_m y)}$. Further, for rotor rows the y-direction of the coordinate was taken the contrary to rotating direction. The relationship between blade fixed coordinate y' and absolute coordinate y is

$$y = y' - \Omega r_m t$$

then the waves in a rotor blade row can be expressed in the form $e^{i(\omega - m\Omega)t + \beta_m y'}$. Using the similar method used in unbladed regions the solution can be obtained in the following form

$$\begin{aligned} p_c^k(x, y', z, t) &= \sum_{m=-\infty}^{+\infty} \sum_{n=1}^{+\infty} (\bar{p}_{mn}^{+k} \psi_{mn}^{+k}(z) e^{i\alpha_{mn}^{+k}(x-x^j)} + \bar{p}_{mn}^{-k} \psi_{mn}^{-k}(z) e^{i\alpha_{mn}^{-k}(x-x^j)}) \times e^{i(\omega - m\Omega)t + i\beta_m y'} \\ \rho_c^k(x, y', z, t) &= \sum_{m=-\infty}^{+\infty} \sum_{n=1}^{+\infty} \left[\frac{1}{a_0^2} (\bar{p}_{mn}^{+k} \psi_{mn}^{+k}(z) e^{i\alpha_{mn}^{+k}(x-x^j)} + \bar{p}_{mn}^{-k} \psi_{mn}^{-k}(z) e^{i\alpha_{mn}^{-k}(x-x^j)}) \right. \\ &\quad \left. + \bar{\rho}_{vmn}^{+k} \psi_{vmn}^{+k}(z) e^{-i\frac{W_c^k \beta_m \sin \theta + (\omega - m\Omega)}{W_c^k \cos \theta} x} \right] \times e^{i(\omega - m\Omega)t + i\beta_m y'} \\ q_c^k(x, y', z, t) &= \sum_{m=-\infty}^{+\infty} \sum_{n=1}^{+\infty} \left[-\frac{1}{\rho_0^k} \left(\frac{\bar{p}_{mn}^{+k} (\alpha_{mn}^{+k} \cos \theta^k + \beta_m \sin \theta^k) e^{i\alpha_{mn}^{+k}(x-x^j)}}{(\omega - m\Omega) + (\alpha_{mn}^{+k} \cos \theta^k + \beta_m \sin \theta^k) W_c^k} \psi_{mn}^{+k}(z) \right. \right. \\ &\quad \left. \left. + \frac{\bar{p}_{mn}^{-k} (\alpha_{mn}^{-k} \cos \theta^k + \beta_m \sin \theta^k) e^{i\alpha_{mn}^{-k}(x-x^j)}}{(\omega - m\Omega) + (\alpha_{mn}^{-k} \cos \theta^k + \beta_m \sin \theta^k) W_c^k} \psi_{mn}^{-k}(z) \right) \right. \\ &\quad \left. + \bar{q}_{vmn}^{+k} \psi_{vmn}^{+k}(z) e^{-i\frac{W_c^k \beta_m \sin \theta + (\omega - m\Omega)}{W_c^k \cos \theta} x} \right] \times e^{i(\omega - m\Omega)t + i\beta_m y'} \\ w_c^k(x, y', z, t) &= \sum_{m=-\infty}^{+\infty} \sum_{n=1}^{+\infty} \left[-\frac{1}{\rho_0^k} \left(\frac{i \bar{p}_{mn}^{+k} k_{mn}^{+k} e^{i\alpha_{mn}^{+k}(x-x^j)}}{(\omega - m\Omega) + (\alpha_{mn}^{+k} \cos \theta^k + \beta_m \sin \theta^k) W_c^k} \phi_{mn}^{+k}(z) \right. \right. \\ &\quad \left. \left. + \frac{i \bar{p}_{mn}^{-k} k_{mn}^{-k} e^{i\alpha_{mn}^{-k}(x-x^j)}}{(\omega - m\Omega) + (\alpha_{mn}^{-k} \cos \theta^k + \beta_m \sin \theta^k) W_c^k} \phi_{mn}^{-k}(z) \right) \right. \\ &\quad \left. + \bar{w}_{vmn}^{+k} \phi_{vmn}^{+k}(z) e^{-i\frac{W_c^k \beta_m \sin \theta + (\omega - m\Omega)}{W_c^k \cos \theta} x} \right] \times e^{i(\omega - m\Omega)t + i\beta_m y'} \end{aligned} \quad (13)$$

In the cases of stator rows rotating speed Ω is set to be 0.

Supersonic Region

For transonic rotor, obviously, the real environments is very complicated. If the presence of shock was ignored the solution of last section can be used directly on transonic rotor with assuming the total pressure loss centralize in the leading edge. But if the shock waves was considered, one simple approach to model them is to treat them as a strong normal in-passage shock. This could be relatively easily modeled in mathematic. The simplified physical sketch is shown in Fig.(2). The blade row channel was separated by the normal shock into two parts, i.e., one supersonic flow field and one subsonic field. Linearized Euler equations, which are the same with last section, will govern the two areas. By solving them respectively two groups of solution could be obtained.

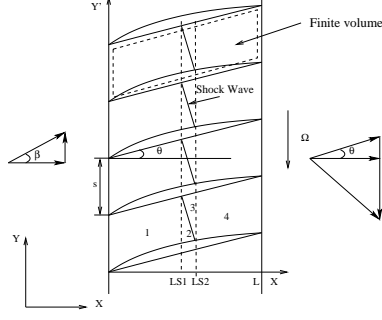


Fig.2: Shock Wave in Rotor Blade Row

It was shown in last section that there are two axial exponential items of acoustic wave mode in a subsonic flow field, one downward and one forward from plane x^j . To supersonic flow field the difference is that only downward perturbation could propagate in it. Therefore, there is only one axial exponential item of acoustic wave mode. As to vortical wave mode and entropy wave mode there is no variance. Hence it is not necessary to write the solution out again. However, it should be noted that it has 3 unknown variables addition to the model with the assumption of existence of a strong normal shock. They are the coefficients of acoustic mode p_{bmn} , vortical mode w_{vbm} and entropic mode ρ_{vbm} , of perturbation of supersonic area.

Matching Condition

In the solutions obtained in last three sections the coefficients of wave mode are unknown. For each disturbance mode there are 5 unknowns in the solution of each unbladed region, 4 unknowns in the solution of each subsonic bladed regions and 3 unknowns in the solution of supersonic bladed region. They could be associated by applying conservation conditions and matching conditions on connected plane, i.e. shock wave, leading edge and trailing edge of blade rows.

Conservation conditions

A finite volume was selected along the blade row channel(see Fig.(2)). The laws of unsteady conservation of mass and energy must be satisfied by the flow of this volume. The equation of unsteady conservation of mass of subsonic cases are

$$\begin{aligned} &(\rho_0^j u^j - \rho_0^{j+1} u^{j+1}) + (\rho^j U^j - \rho^{j+1} U^{j+1}) \\ &- \cos\theta^k \int_0^{c^k} \frac{\partial \rho_c^k}{\partial t} - \rho_0^k c^k \cos\theta^k \frac{\partial \omega^k}{\partial z} = 0 \end{aligned} \quad (14)$$

and the equation of unsteady conservation of energy of subsonic cases are

$$\begin{aligned} &\frac{a_0^2}{\kappa-1} \left(\frac{p^j}{\rho_0^j} - \frac{p^j}{\rho_0^j} \right) - W^j (u^j \cos\beta^k + v^j \sin\beta^k) \\ &- \frac{a_0^2}{\kappa-1} \left(\frac{p^{j+1}}{\rho_0^{j+1}} + \frac{\rho^{j+1}}{\rho_0^{j+1}} \right) - W^{j+1} (u^{j+1} \cos\theta^k + v^{j+1} \sin\theta^k) \\ &- \int_0^{c^k} \frac{\partial q_c^k}{\partial t} d\xi - \frac{\int_0^{c^k} \frac{\partial p_c^k}{\partial t} d\xi - a_0^2 \int_0^{c^k} \frac{\partial \rho_c^k}{\partial t}}{(\kappa-1)\rho_0^{j+1} W^{j+1}} = 0 \end{aligned} \quad (15)$$

For supersonic cases the equation of the unsteady conservation of mass is

$$\begin{aligned} &\rho_0^j u^j + U^j \rho^j - \rho_0^{j+1} u^{j+1} + U^{j+1} \rho^{j+1} \\ &- \int_0^{LS1} \rho_{0b}^k \frac{\partial w_b^k}{\partial z} dx - \int_{LS1}^{LS2} \rho_{0b}^k \frac{\partial w_b^k}{\partial z} \frac{LS2-x}{LS2-LS1} dx \\ &- \int_{LS2}^L \rho_{0a}^k \frac{\partial w_a^k}{\partial z} dx - \int_{LS1}^{LS2} \rho_{0a}^k \frac{\partial w_a^k}{\partial z} \frac{x-LS1}{LS2-LS1} dx \\ &- \frac{\partial}{\partial t} \left\{ \int_0^{LS1} \rho_{cb}^k dx + \int_{LS1}^{LS2} \rho_{cb}^k \frac{LS2-x}{LS2-LS1} dx \right. \\ &\left. + \int_{LS2}^L \rho_{ca}^k dx + \int_{LS1}^{LS2} \rho_{ca}^k \frac{x-LS1}{LS2-LS1} dx \right\} = 0 \end{aligned} \quad (16)$$

and the equation of unsteady conservation of energy is

$$\begin{aligned} &\frac{a_0^2}{\kappa-1} \left(\frac{p^j}{\rho_0^j} - \frac{p^j}{\rho_0^j} \right) + (u^j U^j - v^j V^j) \\ &- \frac{a_0^2}{\kappa-1} \left(\frac{p^{j+1}}{\rho_0^{j+1}} - \frac{p^{j+1}}{\rho_0^{j+1}} \right) - (u^{j+1} U^{j+1} - v^{j+1} V^{j+1}) \\ &= \frac{\partial}{\partial t} \left\{ \int_0^{LS1} \left(q_b^k + \frac{1}{\rho_0^j U^j} \frac{1}{\kappa-1} (p_{0b}^k - a_{0b}^2 \rho_{0b}^k) \right) dx \right. \\ &+ \int_{LS1}^{LS2} \left(q_b^k + \frac{1}{\rho_0^j U^j} \frac{1}{\kappa-1} (p_{0b}^k - a_{0b}^2 \rho_{0b}^k) \right) \frac{LS2-x}{LS2-LS1} dx \\ &+ \int_{LS1}^{LS2} \left(q_a^k + \frac{1}{\rho_0^j U^j} \frac{1}{\kappa-1} (p_{0a}^k - a_{0a}^2 \rho_{0a}^k) \right) \frac{x-LS1}{LS2-LS1} dx \\ &\left. + \int_{LS2}^L \left(q_a^k + \frac{1}{\rho_0^j U^j} \frac{1}{\kappa-1} (p_{0a}^k - a_{0a}^2 \rho_{0a}^k) \right) dx \right\} \end{aligned} \quad (17)$$

This two equations are the main difference resulted by the assumption about the in-passage shock. For the first case, i.e., ignoring the presence of shock, the equations are simpler than equations for the second case. Detailed deduction of unsteady equations can be seen in reference(Sun,1996).

Leading Edge of Blade Rows

The assumption applied in this model is that the blade profile loss is concentrated on the leading edge of blade rows. Hence, an unsteady total pressure loss equation can be set up as

$$\begin{aligned} h_L^j - h_L^k &= \xi_s^k (U^j u^j + V^j v^j) \\ &+ \xi_s^{k'} \frac{(U^j)^2 + (V^j)^2}{2} \left(\frac{v^j}{V^j} - \tan\beta^k \frac{u^j}{U^j} \right) \end{aligned} \quad (18)$$

Although the mean flow turns in the lead edge and the total pressure loss arises there, the momentum in the span wise direction should be continuous because there is no force acting in this direction. Since the mass flow is conserved on the leading edge plane, this condition finally becomes equivalent to the conservation of the fluctuating velocity in this direction, i.e.

$$w^j = w^k \quad (19)$$

Trailing Edge of Blade Rows

On the trailing edge plane, the conservation of mass flow and total enthalpy flow are imposed. In principle the outlet angle from the blade row β_2 is generally given as a function of the inlet flow angle β_1 and the span wise position z. For simplicity it is assumed here that β_2 is constant being independent of β_1 and z. Its value is assumed to be equal to the cascade stagger angle θ . Then the three components of the velocity, static pressure and density are continuous. These conditions will result in the following different algebra equations for a blade row.

The outlet pressure condition is

$$p_c^k = p^{j+1} \quad (20)$$

The outlet density condition is

$$\rho_c^k = \rho_{j+1} \quad (21)$$

The outlet axial velocity condition is

$$q_c^k \cos\theta^k = u^{j+1} \quad (22)$$

The outlet circumferential velocity condition is

$$q_c^k \sin\theta^k = v^{j+1} \quad (23)$$

The outlet radial velocity condition is

$$w_c^k = w^{j+1} \quad (24)$$

Matching Condition on Shock Wave

The semi-actuator theory assumed that all variables had no variation in the direction vertical to the chord direction. Therefore the complicated shock waves inside of rotor blade row were replaced by a normal shock wave for simplicity. Then the relationship of disturbances can be obtained by linearizing the well known normal shock wave relationship.

The radial velocity condition on shock wave is

$$w_a^k = w_b^k \quad (25)$$

The axial velocity condition on shock wave is

$$q_a^k = \frac{(\kappa-1)Ma_b^2-2}{(\kappa+1)Ma_b^2} q_b^k - \frac{2a_0^2}{(\kappa+1)W_b\rho_0^k} \rho_b^k + \frac{2a_0^2}{(\kappa+1)W_b P_b} P_b^k \quad (26)$$

The pressure condition on shock wave is

$$p_a^k = -\frac{\kappa-1}{\kappa+1} p_b^k + \frac{2W_b^2}{\kappa+1} \rho_b^k + \frac{4\rho_0^k W_b}{\kappa+1} q_b^k \quad (27)$$

Inlet and Outlet Conditions of Compressor

Assume that there are no inlet disturbances caused by entropy and vortex and no reflection, so for the first blade row,

$$\bar{p}_{mn}^{+1}, \bar{\rho}_{mn}^{+1}, \bar{v}_{mn}^{+1}, \bar{w}_{mn}^{+1} = 0 \quad (28)$$

On the other hand, for the outlet of compressor, it is assumed that there is no reflection, so

$$\bar{p}_{mn}^N = 0 \quad (29)$$

All equations then were stacked row by row. By use of the boundary condition a homogeneous system of equations with homogeneous boundary condition was obtained. The only thing left is to substitute perturbation solutions of unbladed area and bladed area into these equations. The final form of the equation is like

$$\begin{bmatrix} a_1 & a_2 & \cdots & a_n \\ b_1 & b_2 & \cdots & b_n \\ \vdots & \vdots & \ddots & \vdots \\ l_1 & l_2 & \cdots & l_n \end{bmatrix} \begin{bmatrix} p_{mn}^{+1} \\ p_{mn}^{-1} \\ \vdots \\ \rho_{vmn}^N \end{bmatrix} = \begin{bmatrix} 0 \\ 0 \\ 0 \\ 0 \end{bmatrix} \quad (30)$$

The order of the system of equation depends on the number of rows and the assumption about the shock. If shock is passed over the matching condition on shock will be left out, otherwise the stability equations will have three more equations and three more unknown coefficients related to the supersonic region.

In order to get nontrivial solutions from the equations the determinant of the coefficient matrix must be not equal to zero. Hence allowable frequency ω should be found out in complex field to satisfy this requirement. Recall that the imaginary part of ω will determine whether the flow is stable or unstable.

Result Discussion

As mentioned in introduction, this stability theory needs compressor's performance data, which come from experiment or numerical calculation. At present, experimental data appears to be more accurate than numerical calculation, and in this paper, experimental data was used for this reason. The next subsection describes briefly the experiment. The results of the model and some discussion is in the second subsection.

Performance of One Transonic Stage

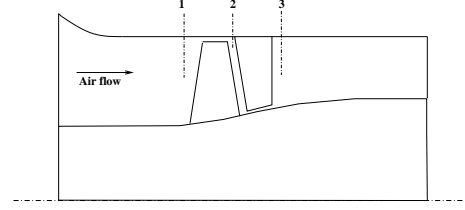


Fig.3: Sketch of the compressor

The experiment quoted in this paper is by Royce(1982), and details of the stage could be obtained by Urasek(1972). Fig.(3) is a sketch of the compressor stage. This stage was designed for a pressure ratio of 1.82 at a flow 20.2 kilograms per second and a tip speed of 455 meters per second. Table.(1) shows some design overall parameters and some geometric data.

Table 1: Design Overall Parameters for Stage

Rotor Total Pressure Ratio	1.863
Stage Total Pressure Ratio	1.820
Rotor Adiabatic Efficiency	0.858
Stage Adiabatic Efficiency	0.822
Flow Coefficient	0.447
RPM	17140
Tip Speed	455.233
Hub-Tip Radius Ratio	0.70
Number of Rotor Blades	48
Number of Stator Blades	62

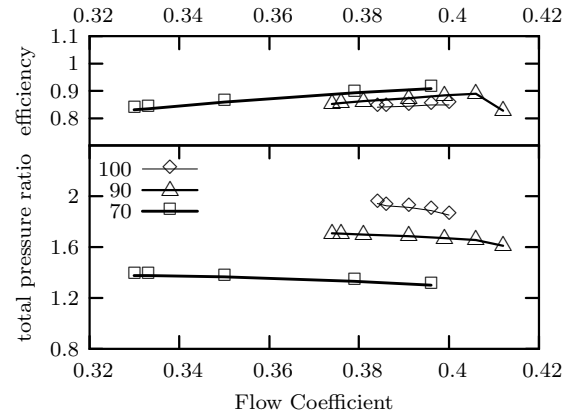


Fig.4: Sketch of performance of the stage

This compressor was tested over the stable operating flow range from 50 to 100 percent of design speed. Fig.(4) gives out the brief performance line of this compressor stage in form of total pressure ratio and efficiency. The relative velocity of flow in the rotor is supersonic when the rotor rotates in 100% design rotating speed, and strong in-passage shock waves exist in the rotor till the compressor goes into stall. Some weak shock waves, the impact of which on stability can be ignored, lie in the stator either. In the experiment the total pressure loss of rotor was measured, but the shock

wave loss was unable to be measured directly in experiment. The relationship among total pressure loss coefficient, blade profile loss coefficient and shock loss coefficient are

$$L_{profile\ loss} = L_{total\ loss} - L_{shock\ loss} \quad (31)$$

For the compressor, the total pressure loss of stator is much less than the loss of rotor, and when the rotor rotates in 100% design speed the loss of shock would be much larger than blade profile loss. Therefore the discussion in next subsection would put focuses on the rotor blade row rather than the stator blade row. In addition, because the main flow in the model was assumed to be two-dimensional so it is necessary to take radial average of the experimental data which were radially distributed in report(Royce,1982).

Numerical Results

There are two different ways to predict the inception of stall in a multi blade rows compressor. One way is to build the stability equations on each row and solve them one by one to find the most unstable point, and the second way is to set up the stability equation on the whole compressor and solve only one system equations. The defect of the first way is that it is difficult to determine the boundary condition of inter-blades. The non-reflection condition at downstream of blade would not be accurate any more. However, this way is still a good attempt, from which some phenomenon and discipline could be found. The second way seems to be closer to the real situation though it also depends on the accuracy of performance data, such as velocity, loss coefficient, and so on. The previous description of this model indicates that if the total pressure loss was assumed to take place just on the leading edge, then the pressure loss of shock would be omitted in conservation laws and matching conditions. This assumption is generally undertaken by most stability theories, so does this paper(See Fig.(5, 6, 7)), moreover, this paper would try to separate the loss of shock from other types of losses and discuss its impact on system stability(See Fig.(8, 9)).

All of the following figures would show relative propagation speed and damping of the disturbance, and the rotor speed is 100% design speed. Their definitions are as follows separately

$$\frac{\omega_r}{2m\pi\Omega}, \quad \frac{\omega_i}{2m\pi\Omega}$$

. It is also noted that radial mode number n is set to one, because when just considering solid wall boundary condition mode number larger than one has no practical meaning. In addition, the experimental data was presented over the stable operating flow range, so it means that the real flow is stable. In order to get the performance data of a possible stall's condition, a little smaller airflow was assumed and was extrapolated from the near stall point. Therefore, in following figures the point with the smallest flow coefficient would be a possible unstable condition.

Ignoring shock would make matching conditions on shock be passed over, correspondingly, unsteady equation of conservation of mass(Eq.(14)) and energy(Eq.(15))are adopted.

Fig.(5) shows four different circumferential mode number for the rotor row, which means the stability equation would be built on rotor only. From this figure, it could be seen that the damping reduces while the airflow decreases, and when the airflow decreases to the near stall condition there is a more sharp decrease in the damping very close to zero, so it is possible that disturbance wave with circumferential mode number 4 and 5 would go into rotating stall.

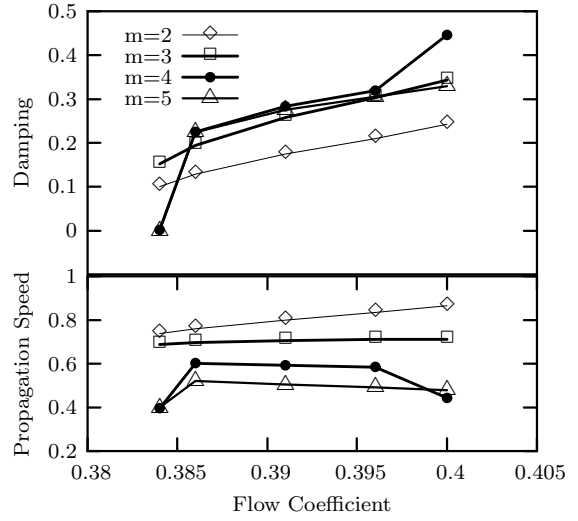


Fig.5: Disturbance wave in rotor

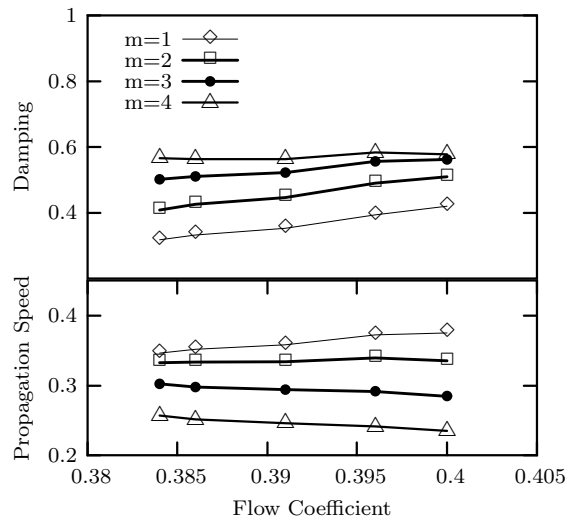


Fig.6: Disturbance wave in stator

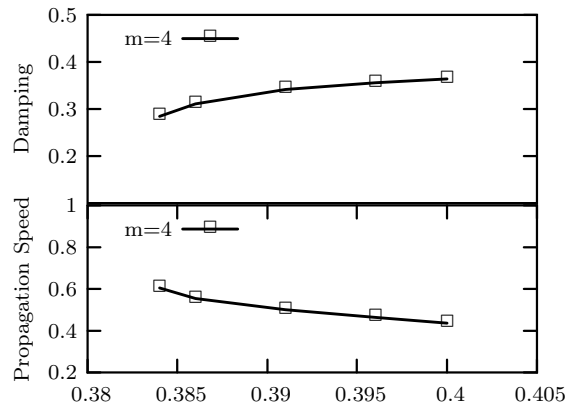


Fig.7: Disturbance wave in stage

Fig(6) is the result built on stator row only. Both of the propagation speed and damping lines are quite flat with the decrease of flow coefficient. Actually, the total pressure loss in the stator is much less than in the rotor. The result of Fig.(7) is built on the stage, namely, rotor and stator. Only the line of circumferential mode number 4 is drawn in the figure. Besides mode number 4 the other mode also had been calculated, but results are not as resonable as circumferential mode number 4, such as a negative propagation speed or a very larger speed than rotative speed.

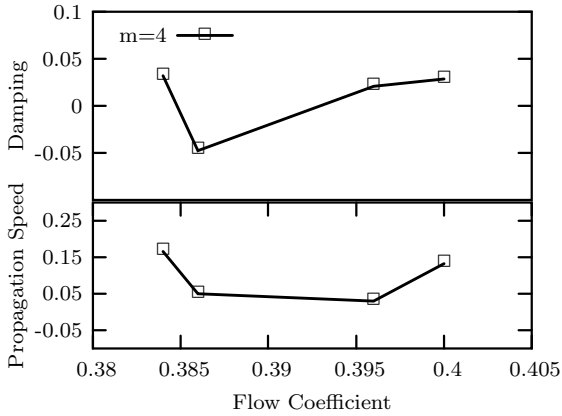


Fig.8: Disturbance wave in rotor

The next is to use matching conditions on shock and unsteady equations of conservation of mass(Eq.(16) and energy(Eq.(17)) in setting up the stability equation. Fig.(8) shows results for rotor, circumferential mode number 4 only. It is noted that the in-passage shock is assumed to be near the leading edge of rotor, because there is no any measurement on it in experiment. Comparing Fig.(5) and Fig.(8) could find that propagation speed of disturbance in the second figure is less than the first one, and the same trend lies in the damping lines. Another difference is that in the first case the damping is close to zero at the point of the smallest airflow, while in the second case the damping has been less than zero at the flow nearly stall. Results in Fig.(9) are similar with Fig.(7). Both of them were obtained by applying the model to the whole stage. Comparison between them shows that the propagation speed of disturbance wave in view of shock is less than the other, and the trend of damping is more resonable.

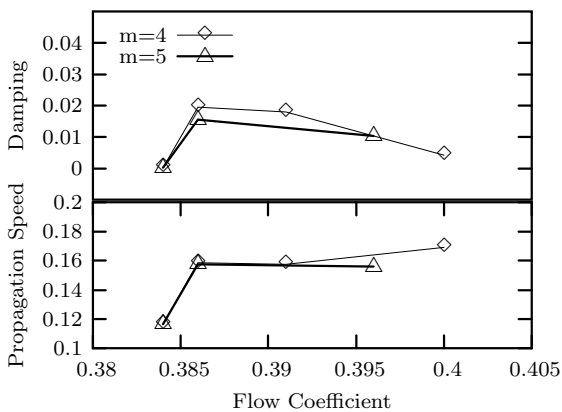


Fig.9: Disturbance wave in stage

So the first conclusion could be drawn is that circumferen-

tial mode number 4 or 5 are the most possible modes which might go into rotating stall. The second conclusion is that comprising the shock in model has a positive impact on result. This was embodied not only in the result for one blade row but also the whole stage. Considering shock in model actually increases the order of coefficient matrix of stability equations, and it would reduce the blade profile loss coefficient and its derivative to inlet angle either. It had been emphasized by Nenni and Ludwig(1974) in their subsonic model that the loss coefficient and its derivative to inlet swirl are the most important factor on stability of compressor. This point is widely accepted no matter the flow is compressible or incompressible. As mentioned previously, blade profile loss is obtained by subtracting the shock loss from the total pressure loss. When in-passage shock exists, because the blade profile loss is much less than shock loss, its derivative to inlet swirl would become much less than the usual subsonic condition correspondingly. Though a direct measurement on shock could not be obtained in experiment, but from the existing experimental data this is true. The sharp variance of propagation speed and damping in Fig.(8) and Fig.(9) could possibly originate from that the slope of blade profile loss to inlet swirl is not smooth in transonic flow. Anyway, the correlation between the prediction of theory and experiment indicates that the model in view of shock is more accurate and resonable. The third conclusion is that for a multi rows compressor, the results built on the whole stage is more accurate than results built on rotor only, as is shown in Fig.(8, 9). The existence of stator row would probably increase the stability of the stage, and another reason is that it is difficult to give out an accurate boundary condition between the blade rows into the model.

Concluding Remarks

The stability theory of rotating stall of compressors is to help understanding the mechanism of rotating stall in order to find various ways to extend the stall margin. To transonic axial flow compressors or fans, there is very few models to discuss the role of a strong in-passage shock on the stability. Based on an existing compressible rotating stall stability model, a three-dimensional supersonic stability theory of rotating stall has been developed to include the effect of in-passage shock, which is simplified as a normal shock. The present numerical results show that the model in view of shock can give a rather reasonable stability prediction, and the impact of in-passage shock on stability is thought to be resulted from shock pressure loss, which changes the slope of total pressure loss to inlet flow angle. More comparisons between theory and experiment will be done to test the conclusion in the future.

References

- Adamzyck, J. J., 1978, "Analysis of Supersonic Bending Flutter in Axial Flow Compressor by Actuator Disk Theory," NASA TP-1345.
- Feulner, M. R., et al, 1994, "Modeling for Control of Rotating Stall in High Speed Multi-Stage Axial compressors," ASME 94-Gt-2.
- Greitzer, E. M., 1976, "Surge and Rotating Stall in Axial Flow Compressors," Part1-Part2, Trans.ASME, Journal of Engineering for Power, Vol.98, pp.190-217.
- Ludwig, G. R., and Nenni, J. P., 1979, "Basic Studies of Rotating Stall in Axial Flow Compressors," AFAPL-TR-79-2083.
- Micklow, J., and Jeffers, J., 1981, "Semi-Actuator Disk Theory for Compressor Choke Flutter," NASA CR-3426.

Moore, F. K., 1984, "A Theory of Rotating Stall of Multistage Axial Compressors," Part1-Part3, Trans.ASME, Journal of Engineering for Gas Turbine and Power, Vol.106, pp.313-334.

Moore, F. K., Greitzer, E. M., 1986, "A Theory of Post-Stall Transients in Axial Compression Systems," Part1-Part2, Trans.ASME, Journal of Engineering for Gas Turbine and Power, Vol.108, pp.68-75, pp.231-239.

Nenni, J. P., and Ludwig, G. R., 1974, "A Theory to Predict the Inception of Rotating Stall in Axial Flow Compressors," AIAA Paper 74-528.

Moore, R. D. and Reid, L., 1982, "Performance of Single-Stage Axial-Flow Transonic Compressor With Rotor and Stator Aspect Ratios of 1.63 and 1.78, Respectively, and With Design Pressure of 1.82," NASA TP-1974.

Sun, X. F., 1996, "Three-Dimensional Compressible Flow Stability Theory of Rotating Stall," BUAA Technical Report, BH-B4765.

Sears, W. R., 1955, "Rotating Stall in Axial Compressors," ZAMP, Vol.6, 1955, pp.429-454.

Takata, H., and Nagano, S., 1970, "Nonlinear Analysis of Rotating Stall," Trans. ASME Series A, vol.94, No.4, pp.279.

Takata, H., and Nagashima, T., 1985b, "Rotating Stall in Three-Dimensional Blade Rows Subjected to Spanwise Shear Flow," ISABE 85-7008, pp.389-405.

Ursek, D. C., and Janetzke, D. C., 1972, "Performance of Tandem-Bladed Transonic Compressor Rotor with Rotor Tip Speed of 1375 Feet Per Second," NASA TM X-2484.